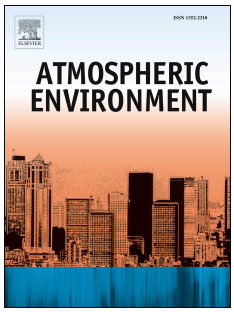

Mixing order of sulfate aerosols and isoprene epoxydiols affect secondary organic aerosol formation in chamber experiments

Theodora Nah, Lu Xu, Kymberlee A. Osborne-Benthaus, S. Meghan White, Stefan France, Nga Lee Ng

PII: S1352-2310(19)30592-8

DOI: https://doi.org/10.1016/j.atmosenv.2019.116953

Reference: AEA 116953

To appear in: *Atmospheric Environment*

Received Date: 29 March 2019

Revised Date: 24 August 2019

Accepted Date: 2 September 2019

Please cite this article as: Nah, T., Xu, L., Osborne-Benthaus, K.A., White, S.M., France, S., Lee Ng, N., Mixing order of sulfate aerosols and isoprene epoxydiols affect secondary organic aerosol formation in chamber experiments, *Atmospheric Environment* (2019), doi: https://doi.org/10.1016/j.atmosenv.2019.116953.

Mixing Order of Sulfate Aerosols and Isoprene Epoxydiols Affect Secondary Organic Aerosol Formation in Chamber Experiments

Theodora Nah,[1,4*] Lu Xu,[1,5] Kymberlee A. Osborne-Benthaus,[2] S. Meghan White,[2] Stefan France[2] and Nga Lee Ng[1,3*]

[1]*School of Chemical and Biomolecular Engineering, Georgia Institute of Technology, Atlanta, GA, USA*
[2]*School of Chemistry and Biochemistry, Georgia Institute of Technology, Atlanta, GA, USA*
[3]*School of Earth and Atmospheric Sciences, Georgia Institute of Technology, Atlanta, GA, USA*
[4]*School of Energy and Environment, City University of Hong Kong, Hong Kong, China*
[5]*Division of Geological and Planetary Sciences, California Institute of Technology, Pasadena, CA, USA*

** To whom correspondence should be addressed:*
Theodora Nah (Postal address: School of Energy and Environment, City University of Hong Kong, Tat Chee Avenue, Kowloon, Hong Kong, China, Email: theodora.nah@cityu.edu.hk, Tel: +852 3442 5578, Fax: +852 3442 0688)
Nga Lee Ng (Postal address: School of Chemical and Biomolecular Engineering, Georgia Institute of Technology, 311 Ferst Drive N.W., Atlanta, Georgia, USA, Email: ng@chbe.gatech.edu, Tel: +1 404 385 2148, Fax: +1 404 894 2866)

Abstract

The reactive uptake of isoprene epoxydiols (IEPOX) is a significant source of isoprene-derived secondary organic aerosols (SOA). Multiple field studies have reported that summertime isoprene-derived SOA in the Southeastern U.S. correlated strongly with sulfate mass concentration. However, previous laboratory studies have focused largely on the effect of aerosol acidity on the reactive uptake of IEPOX. In this study, we investigated the role of inorganic sulfate aerosols in SOA formation arising from the reactive uptake of *trans-β*-IEPOX (the predominant IEPOX isomer) at 50 to 56 % RH in laboratory chamber experiments. Our measurements showed that the SOA mass concentration increased with the sulfate mass for both highly acidic and less acidic seed aerosols. This was due to the roles that sulfate played in SOA formation as a particle-phase reactant and as a contributor to aerosol surface area and volume. Higher concentrations of SOA were formed when highly acidic seed aerosols were used, consistent with previous laboratory studies. SOA mass concentration and composition were also observed to be dependent on the injection order of IEPOX and sulfate seed aerosols (i.e., injection of IEPOX first vs. injection of seed aerosols first) in the chamber experiments. Higher SOA mass concentrations were measured in experiments where sulfate seed aerosols were introduced into the chamber first, followed by IEPOX. Volatility measurements showed that the SOA formed in the "seed aerosols first" experiments likely contained larger quantities of low

volatility organic matter compared to SOA formed in the "IEPOX first" experiments. These results showed that the mass concentration and composition of IEPOX-derived SOA formed in chamber experiments can be sensitive to mixing conditions in the chamber brought about by slight differences in experimental methodology (in this case injection procedure). The sensitivity of SOA formation to the amount of seed aerosols and injection procedure used in chamber experiments indicated that caution should be exercised when extrapolating laboratory data to ambient conditions.

Keywords

Secondary organic aerosols, Isoprene, Reactive uptake, Sulfate, Multiphase chemistry

1. Introduction

Isoprene is the most abundant non-methane biogenic volatile organic compound (BVOC) in the atmosphere, with emissions estimated to be ~535 TgC yr^{-1} (Guenther et al., 2012). The large abundance of isoprene, combined with its high reactivity to various atmospheric oxidants (e.g., OH and NO_3), make it an important component in atmospheric chemistry. The photooxidation of isoprene plays an important role in regulating the cycling of HO_x species (HO_x = OH + HO_2) and tropospheric O_3 production in regions with high isoprene emissions (Thornton et al., 2002; Lelieveld et al., 2008; Ren et al., 2008; Paulot et al., 2009a; Wennberg et al., 2018). Isoprene reacts rapidly with OH radicals (k = 1.0 × 10^{-10} cm^3 $molec.^{-1}$ s^{-1}) via OH addition followed by O_2 addition to form hydroxyl peroxy radicals (Atkinson et al., 2006). In low-NO environments, these hydroxyl peroxy radicals react primarily with HO_2 radicals to form hydroxy hydroperoxides (ISOPOOH), with yields exceeding 80 % (Paulot et al., 2009a; Surratt et al., 2010; Bates et al., 2014; Wennberg et al., 2018). Further reaction of ISOPOOH with OH radicals leads to the formation of isoprene epoxydiols (IEPOX), with yields of 70 to 80 % (Paulot et al., 2009a; Surratt et al., 2010; Bates et al., 2014; Liu et al., 2015; St. Clair et al., 2016; Wennberg et al., 2018). The reactive uptake of IEPOX by aqueous aerosols leads to the formation of secondary organic aerosols (SOA). This occurs through the acid-catalyzed ring-opening of the IEPOX epoxide functional group in concert with the addition of particle-phase nucleophiles (e.g., sulfate and water) to form particle-phase products such as 3-methyltetrahydrofuran-2,4-diols, 2-methyltetrols, oligomers and organosulfates (Wang et al., 2005; Surratt et al., 2007a;

Minerath et al., 2008; Surratt et al., 2008; Carlton et al., 2009; Chan et al., 2010; Eddingsaas et al., 2010; Surratt et al., 2010; Lin et al., 2012; Budisulistiorini et al., 2013; Worton et al., 2013; Nguyen et al., 2014; Rattanavaraha et al., 2016; Riedel et al., 2016; Watanabe et al., 2018). A simplified reaction scheme for the formation of prominent particle-phase IEPOX-derived species is shown in Fig. S1. IEPOX multiphase chemistry contributes a substantial fraction of biogenic SOA in forested regions where anthropogenic pollutants are present (Chan et al., 2010; Budisulistiorini et al., 2013; Lin et al., 2013; Worton et al., 2013; Budisulistiorini et al., 2015; Chen et al., 2015; Hu et al., 2015; Xu et al., 2015a; Xu et al., 2015b; Rattanavaraha et al., 2016; Zhang et al., 2017; Andreae et al., 2018).

To date, most laboratory studies have focused primarily on the effect of aerosol acidity on the reactive uptake of IEPOX. Many of these studies demonstrated that aerosol acidity enhances IEPOX reactive uptake, and consequently SOA formation (Surratt et al., 2007b; Lin et al., 2012; Gaston et al., 2014; Kuwata et al., 2015; Riedel et al., 2016). However, field measurements showed that summertime isoprene-derived SOA in the Southeastern U.S. correlated strongly with sulfate mass concentration (Lin et al., 2013; Budisulistiorini et al., 2015; Xu et al., 2015a; Rattanavaraha et al., 2016). In addition, isoprene-derived SOA formation was observed to be enhanced when isoprene-rich air masses mixed with sulfate-rich plumes emitted by power plants located in the Southeastern U.S. (Xu et al., 2016). The authors suggested that the high sulfate mass concentrations in these plumes increased both the IEPOX heterogeneous uptake rate (through aerosol surface area) and particle-phase reaction rates (through aerosol acidity), leading to increased isoprene-derived SOA formation. Other studies suggested that the association between isoprene-derived SOA and sulfate mass concentration could arise from the nucleophilic and/or the salting in effects of sulfate (Nguyen et al., 2014; Xu et al., 2015a; Sareen et al., 2017; Nestorowicz et al., 2018), and the increase in aerosol volume concentrations brought about by sulfate enhancement (Lin et al., 2013; Riva et al., 2016). Weak correlations between isoprene-derived SOA and aerosol acidity in the Southeastern U.S. were attributed to aerosol acidity not being a limiting factor due to the highly acidic nature of Southeastern U.S. aerosols (pH 0 to 2) (Guo et al., 2015; Xu et al., 2015a; Weber et al., 2016). Despite ambient measurements showing strong correlations between isoprene-derived SOA and sulfate mass concentration, the relationship between sulfate mass and IEPOX-derived SOA mass concentration has not been examined systematically in laboratory studies.

Many chamber studies that investigate SOA formation from the uptake of a reactive gas onto seed aerosols typically introduce seed aerosols into the chamber before the reactive gas. In addition to the reactive uptake of IEPOX (Lin et al., 2012; Nguyen et al., 2014; Riedel et al., 2015; Riva et al., 2016), other examples of such chamber studies include the reactive uptake of carbonyls, olefins and epoxides onto inorganic seed aerosols (Kroll et al., 2005; Liggio and Li, 2006, 2008; Iinuma et al., 2009; De Haan et al., 2018). It is currently unclear if the injection order of seed aerosols and the reactive gas will affect mixing conditions in the chamber, and consequently affect the amount of SOA and types of products formed.

In this study, we investigate how sulfate mass concentration affects SOA formation from the reactive uptake of IEPOX by inorganic sulfate aerosols of different aerosol acidity at 50 to 56 % RH in chamber experiments. We then expand on this work and explore how the IEPOX-derived SOA mass concentration, composition, and volatilities of particle-phase products formed depend on how acidic seed aerosols and IEPOX are mixed in the chamber by varying the injection order of IEPOX and seed aerosols into the chamber.

2. Materials and methods

Experiments were conducted in the Georgia Tech Environmental Chamber (GTEC) facility, which consists of two 13 m^3 Teflon chambers (Boyd et al., 2015). A synthesized *trans-β*-IEPOX standard was used in this study. The synthesis procedure, which was adapted from previous procedures by Zhang et al. (2012) and Bates et al. (2014), is detailed in the Supplementary Information (SI), and produced a *trans-β*-IEPOX standard of ~96 % purity as determined by nuclear magnetic resonance (NMR) spectroscopy (Figs. S2 and S3). Since the synthesized *trans-β*-IEPOX standard was viscous, it was diluted with ethyl acetate to a concentration of 0.1 g mL^{-1} (after accounting for purity) so that it could be drawn with a syringe for use in chamber experiments. Control experiments were performed to ensure that ethyl acetate did not contribute to SOA formation. All experiments were run at 50 to 56 % RH at room temperature (25 °C). Before each experiment, the chamber was flushed continuously with purified air for at least 36 h.

Aerosol size distributions, number and volume concentrations were measured by a Scanning Mobility Particle Sizer (SMPS, TSI), consisting of a Differential Mobility Analyzer

(DMA, TSI 3081) and a Condensation Particle Counter (CPC, TSI 3775). The bulk aerosol elemental composition and SOA mass concentration was measured by a High-Resolution Time-of-Flight Aerosol Mass Spectrometer (HR-ToF-AMS, Aerodyne Research Inc.) (DeCarlo et al., 2006; Canagaratna et al., 2015). Uncertainties in the HR-ToF-AMS measurements were estimated to be approximately 38 % (Bahreini et al., 2009). Aerosols were not dried prior to being sampled by the HR-ToF-AMS. Thus, the aerosols likely have a high water content, and consequently a low bounce probability in the HR-ToF-AMS (Matthew et al., 2008; Docherty et al., 2013). It is possible that the use of different types of seed aerosols and the products formed in the experiments may result in changes in the collection and ionization efficiencies of the HR-ToF-AMS. However, we were unable to determine the magnitude of these changes. Hence, for simplicity, we assumed that the collection and ionization efficiencies of the HR-ToF-AMS did not change during the study. Gas-phase IEPOX and products evaporated from aerosols during the reactive uptake of IEPOX by sulfate seed aerosols were measured by a High-Resolution Time-of-Flight Chemical Ionization Mass Spectrometer (HR-ToF-CIMS, Aerodyne Research Inc.) using iodide as the reagent ion (Bertram et al., 2011; Lee et al., 2014). These gas-phase species were detected in the form of iodide adducts (Lopez-Hilfiker et al., 2016).

In selected experiments, a Filter Inlet for Gases and AEROsols (FIGAERO, Aerodyne Research Inc.) was coupled to the HR-ToF-CIMS to measure the molecular composition and volatilities of particle-phase products (Lopez-Hilfiker et al., 2014). This instrument combination is referred to hereafter as the FIGAERO-CIMS. Aerosols were collected onto a PTFE filter (Pall Corp, Zefluor 25 mm, 1 μm pore-size) for 5 min while gas-phase species were being sampled and analyzed. The collected aerosols were then thermally desorbed in ultra-high purity (UHP) N_2. The UHP N_2, which was delivered at 2 L min^{-1} across the PTFE filter, was gradually heated at 30 °C min^{-1} from 25 to 200 °C, and then held at 200 °C for 10 min to ensure that all the organic matter was removed from the filter. Organic vapors produced during the thermal desorption process were measured as a function of desorption temperature by the HR-ToF-CIMS, generating a thermogram (i.e., desorption signal vs. desorption temperature) for individual particle-phase species of a given ion elemental composition. Previous studies have shown that the maximum desorption temperature (T_{max}) of an organic compound correlates with its enthalpy of sublimation and saturation vapor pressure (Lopez-Hilfiker et al., 2014; Mohr et al., 2017). Hence, we used multicomponent mixtures comprised of organic compounds of known

157 saturation vapor pressures to calibrate the desorption temperature axis. Figure S4 shows the
158 literature vapor pressures of these organic compounds (Table S1) as a function of their measured
159 T_{max} values. T_{max} values of thermograms of individual particle-phase products measured during
160 chamber experiments were then compared against the calibration desorption temperature axis
161 (Fig. S4) to infer the vapor pressures of these products.

162 The ion signals of gas- and particle-phase species measured in experiments were
163 normalized against the iodide reagent ion (I^-) signal. Due to the commercial unavailability of the
164 gas- and particle-phase products formed from IEPOX reactive uptake, the HR-ToF-CIMS was
165 not calibrated for these compounds, and concentrations were not reported. However, the HR-
166 ToF-CIMS and FIGAERO-CIMS data were used for the identification of gas- and particle-phase
167 products formed under different experimental conditions.

168 Two sets of experiments were used to study SOA formation from the reactive uptake of
169 IEPOX: "IEPOX first" and "seed aerosols first". In both sets of experiments, a known volume of
170 the diluted *trans-β*-IEPOX standard was injected into a gently heated glass bulb (~55 °C). The
171 IEPOX vapor was carried into the chamber using 5 L min^{-1} of purified air until all the IEPOX
172 standard in the glass bulb have evaporated (~2.5 h). The concentration of IEPOX in the chamber
173 (65 ppb ≈ 314 μg m^{-3}) was calculated from the mass of IEPOX injected (~4.1 mg) and the
174 volume of the chamber. Note that this calculated IEPOX concentration assumes that the loss of
175 IEPOX to the chamber walls is negligible. Non-acidified or acidified sulfate seed aerosols were
176 used in these experiments. Non-acidified sulfate seed aerosols were produced by atomization of a
177 0.005 M ammonium sulfate (AS) solution. Acidified sulfate seed aerosols were generated by
178 atomization of a 0.005 M AS solution mixed with different concentrations of sulfuric acid (SA):
179 0.005 M, 0.05 M and 0.1 M. Acidified sulfate seed aerosols will be referred to hereafter by the
180 solutions' molar concentration ratios of sulfuric acid and ammonium sulfate ([SA]/[AS]). For
181 example, seed aerosols generated by a 0.005 M AS + 0.1 M SA solution are referred to as
182 [SA]/[AS] = 20 seed aerosols. In "IEPOX first" experiments, IEPOX was introduced into the
183 chamber first. Seed aerosols were then introduced into the chamber after the IEPOX signal
184 measured by the HR-ToF-CIMS had stabilized. In "seed aerosols first" experiments, seed
185 aerosols were introduced into the chamber first. IEPOX was then introduced into the chamber
186 after the concentration of seed aerosols measured by the SMPS had stabilized. Estimates of the

187 acidity of seed aerosols were obtained using ISORROPIA II (Fountoukis and Nenes, 2007).
188 Experimental conditions are summarized in Table 1.

189 **Table 1:** Experimental conditions for *trans-β*-IEPOX uptake experiments[a]

Expt	RH (%)	Seed aerosols[b]	Injection order	$[SO_4]$ ($\mu g\ m^{-3}$)[e]	Aerosol surface area conc. ($\mu m^2\ cm^{-3}$)[f]	Aerosol volume conc. ($\mu m^3\ cm^{-3}$)[g]
1	56	[SA]/[AS] = 10 (pH = -0.82)	IEPOX first[d]	19.4±0.3	(18.8±0.3) x10^2	57.8±0.6
2	53	[SA]/[AS] = 10 (pH = -0.84)	Seed aerosols first[d]	21.0±0.3	(20.3±0.3) x10^2	57.9±0.5
3	50	AS (pH = 3)	IEPOX first[c]	5.9±0.1 to 35.0±0.1	(58.0±0.5) x10 to (26.6±0.6) x10^2	17.5±0.4 to 82.9±0.9
4	50	[SA]/[AS] = 1 (pH = 0.40)	IEPOX first[c]	13.8±0.7 to 37.5±1.3	(12.8±0.6) x10^2 to (29.0±0.9) x10^2	50±3 to 122±4
5	52	[SA]/[AS] = 10 (pH = -0.85)	IEPOX first[c]	19.3±0.5 to 46.5±1.1	(15.4±0.4) x10^2 to (31.3±0.7) x10^2	52.5±0.9 to 112±2
6	51	[SA]/[AS] = 20 (pH = -0.90)	IEPOX first[c]	8.8±0.1 to 40.0±0.4	(89.3±0.5) x10 to (30.5±0.3) x10^2	27.8±0.1 to 99.4±0.7
7	50	[SA]/[AS] = 10 (pH = -0.87)	IEPOX first[d]	6.0±0.4	(64.1±0.3) x10	18.2±0.6
8	53	[SA]/[AS] = 10 (pH = -0.84)	Seed aerosols first[d]	5.2±0.1	(53.1±0.7) x10	13.4±0.4
9	52	[SA]/[AS] = 10 (pH = -0.85)	IEPOX first[d]	13.8±0.3	(14.8±0.3) x10^2	43.2±0.5
10	52	[SA]/[AS] = 10 (pH = -0.84)	Seed aerosols first[d]	12.5±0.2	(12.4±0.2) x10^2	33.8±0.4

190 [a]~4.1 mg of *trans-β*-IEPOX was injected into the chamber in all experiments.
191 [b]pH values of seed aerosols were estimated using ISORROPIA-II run in "forward" mode with
192 experimental conditions as model inputs.
193 [c]Experiment involved multiple injections of seed aerosols.
194 [d]Experiment involved a single injection of seed aerosols.
195 [e]$[SO_4]$ reported for experiments 1, 3 to 7, and 9 are concentrations measured by the HR-ToF-
196 AMS after IEPOX reactive uptake upon the addition of seed aerosols, and includes both
197 inorganic sulfate from the seed aerosols and organic sulfate formed during SOA formation. $[SO_4]$
198 reported for experiments 2, 8, and 10 are concentrations measured before IEPOX was added into
199 the chamber.
200 [f]Aerosol surface area concentrations reported for experiments 1, 3 to 7, and 9 are those measured
201 by the HR-ToF-AMS after IEPOX reactive uptake upon the addition of seed aerosols. Aerosol
202 surface area concentrations reported for experiments 2, 8, and 10 are those measured before
203 IEPOX was added into the chamber.
204 [g]Aerosol volume concentrations reported for experiments 1, 3 to 7, and 9 are those measured
205 after IEPOX reactive uptake upon the addition of seed aerosols. Aerosol volume concentrations

reported for experiments 2, 8, and 10 are those measured before IEPOX was added into the chamber.

Comparisons of SOA formed from "IEPOX first" and "seed aerosols first" experiments require knowledge of the rate at which IEPOX is lost to the chamber walls and how this may affect SOA formation during an experiment. A wall loss experiment was performed to characterize the interactions of IEPOX with the chamber walls. IEPOX was injected into the chamber in the absence of seed aerosols at 55 % RH, and the gas-phase IEPOX ($C_5H_{10}O_3$) signal was measured by the HR-ToF-CIMS as a function of time (Fig. S5). The negligible decrease in the IEPOX signal in our wall loss experiments suggest that the loss of IEPOX to the chamber walls would be negligible in the timescale of our IEPOX reactive uptake experiments (3 to 5 h). The possibility of IEPOX loss to the chamber walls will be discussed further in the next section.

3. Results and discussion

The highest HR-ToF-CIMS gas- and particle-phase ion signals in all "IEPOX first" and "seed aerosols first" experiments were $C_5H_{10}O_3$ and $C_5H_{12}O_4$, which together contributed ~99 % of the total ion signal. These two ions were the dominant ions measured in a previous chamber study that investigated the reactive uptake of an IEPOX standard (Lopez-Hilfiker et al., 2016). These two ions also dominated the sum of HR-ToF-CIMS ion signals attributed to isoprene-derived SOA measured during the Southern Oxidant and Aerosol Study (SOAS) campaign (Lopez-Hilfiker et al., 2016). Since the other mass ions in our HR-ToF-CIMS measurements have very low signals, we will restrict our discussion to the evolution of the $C_5H_{10}O_3$ and $C_5H_{12}O_4$ signals.

Figures 1a and 1b show typical time profiles of gas-phase $C_5H_{10}O_3$ and $C_5H_{12}O_4$ species measured by the HR-ToF-CIMS during an "IEPOX first" (experiment 1) and "seed aerosols first" (experiment 2) experiment, respectively. The corresponding time profiles of aerosol mass concentrations of organic and sulfate species measured by the HR-ToF-AMS are shown in Figs. 1c and 1d. During the "IEPOX first" experiment, the $C_5H_{10}O_3$ signal decreased while the $C_5H_{12}O_4$ signal increased when seed aerosols were introduced into the chamber at time = 0 min (Fig. 1a). The introduction of seed aerosols into the chamber containing IEPOX brought about immediate SOA formation as shown by the increase in aerosol organic mass concentration (Fig. 1c). During the "seed aerosols first" experiment, the $C_5H_{10}O_3$ and $C_5H_{12}O_4$ signals increased

when IEPOX was introduced into the chamber at time = 0 min (Fig. 1b). The introduction of IEPOX into the chamber containing seed aerosols also resulted in immediate SOA formation (Fig. 1d).

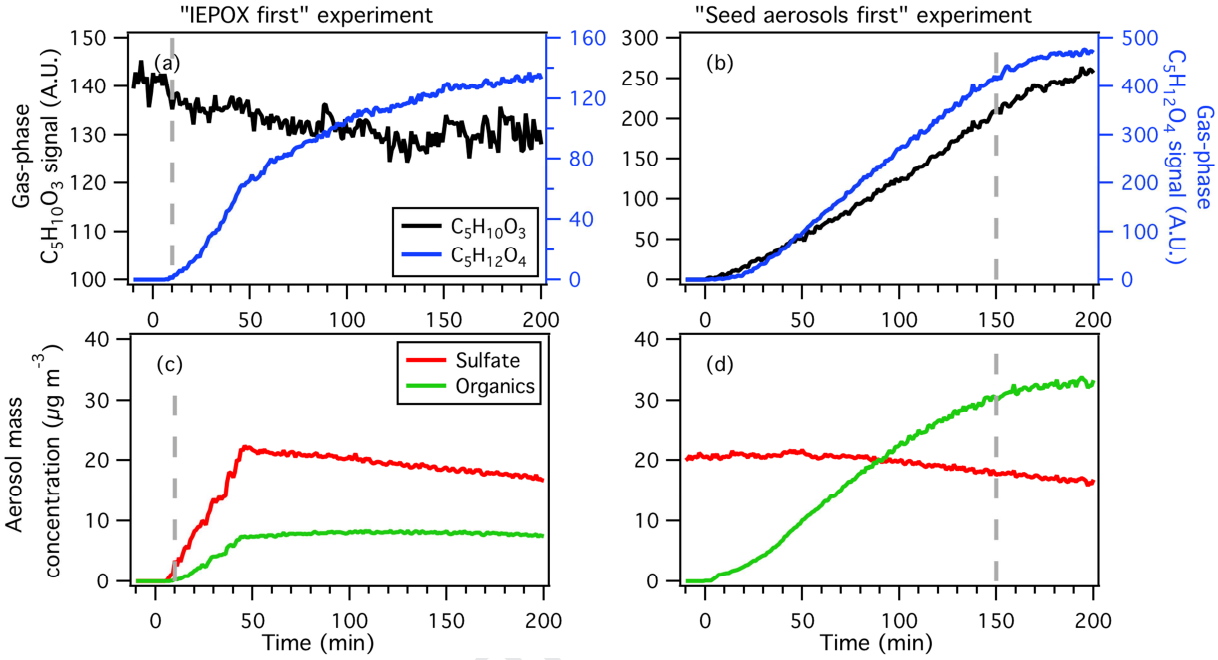

Figure 1: Time series of quantities measured in *trans*-β-IEPOX uptake experiments using [SA]/[AS] = 10 seed aerosols. Panels (a) and (c) show a time series from an "IEPOX first" experiment (experiment 1 in Table 1), where seed aerosols are injected into the chamber at time = 0 min and ended at time = 10 min (indicated by grey dashed line). Panels (b) and (d) show a time series from a "seed aerosols first" experiment (experiment 2 in Table 1), where IEPOX is injected into the chamber at time = 0 min and ended at time = 150 min (indicated by grey dashed line). (a) and (b) Gas-phase $C_5H_{10}O_3$ and $C_5H_{12}O_4$ measured by the HR-ToF-CIMS. In both panels (a) and (b), $C_5H_{10}O_3$ is shown on the left y axis, while $C_5H_{12}O_4$ is shown on the right y axis. (c) and (d) Mass concentrations of organics and sulfate measured by the HR-ToF-AMS.

In addition to the injected IEPOX contributing to the $C_5H_{10}O_3$ signal, the gas-phase $C_5H_{10}O_3$ and $C_5H_{12}O_4$ signals can be explained by the evaporation of semi-volatile particle-phase products from IEPOX-derived SOA. Previous laboratory studies have identified $C_5H_{10}O_3$ and $C_5H_{12}O_4$ as common molecular tracers found in SOA formed from the reactive uptake of IEPOX by inorganic sulfate aerosols (Lin et al., 2012; Lin et al., 2013; Lopez-Hilfiker et al., 2016; Riedel et al., 2016). These studies reported that particle-phase $C_5H_{10}O_3$ species can be comprised of IEPOX itself and 3-methyltetrahydrofuran-2,4-diols, while particle-phase $C_5H_{12}O_4$ can be comprised of 2-methyltetrols. 2-Methyltetrols and 3-methyltetrahydrofuran-2,4-diols are formed

by nucleophilic addition and isomerization reactions, respectively, following the reactive uptake of IEPOX by inorganic sulfate aerosols (Surratt et al., 2010; Watanabe et al., 2018). In studies that utilized FIGAERO-CIMS and other similar thermal desorption-based techniques, a fraction of the measured particle-phase $C_5H_{10}O_3$ and $C_5H_{12}O_4$ signals are attributed to molecular fragments produced by the decomposition of low volatility particle-phase products during the thermal desorption process (Lopez-Hilfiker et al., 2016; Cui et al., 2018).

2-Methyltetrols and 3-methyltetrahydrofuran-2,4-diols are semi-volatile species. Hence, the measured gas-phase $C_5H_{12}O_4$ species in this study were likely 2-methyltetrols that evaporated from the SOA formed. The gas-phase $C_5H_{12}O_4$ signal immediately increased upon the addition of seed aerosols and IEPOX in "IEPOX first" and "seed aerosols first" experiments, respectively. This implied that the heterogenous uptake of IEPOX and subsequent formation of semi-volatile particle-phase products followed by evaporation to the gas phase was fast. A higher gas-phase $C_5H_{12}O_4$ signal was measured in the "seed aerosols first" experiment.

For the measured gas-phase $C_5H_{10}O_3$ species in "IEPOX first" experiments, they were solely IEPOX before the addition of seed aerosols, but were likely a mixture of IEPOX and 3-methyltetrahydrofuran-2,4-diols after the addition of seed aerosols. In the case of "seed aerosols first" experiments, the measured gas-phase $C_5H_{10}O_3$ species were likely a mixture of IEPOX and 3-methyltetrahydrofuran-2,4-diols once IEPOX was injected into the chamber. The HR-ToF-CIMS cannot resolve the structural isomers of $C_5H_{10}O_3$ (i.e., IEPOX vs. 3-methyltetrahydrofuran-2,4-diols), which can have different sensitivities to the iodide reagent ion due to differences in the molecular geometry and functional groups present. Thus, we were unable to determine the relative contributions of IEPOX and 3-methyltetrahydrofuran-2,4-diols to the measured gas-phase $C_5H_{10}O_3$ signal.

Even though the same mass of IEPOX was injected in the "IEPOX first" and "seed aerosols first" experiments, a higher gas-phase $C_5H_{10}O_3$ signal was measured at the end of the "seed aerosols first" experiment (~250 A.U. in Fig. 1b) compared to the $C_5H_{10}O_3$ signals measured prior to (~140 A.U. in Fig. 1a) and after (~130 A.U. in Fig. 1a) the addition of seed aerosols in the "IEPOX first" experiment. Similar trends were observed in the other "IEPOX first" (experiments 7 and 9) and "seed aerosols first" (experiments 8 and 10) experiments. There are two possible explanations for this observation. First, it is possible that despite the negligible

decrease in the IEPOX signal in our wall loss experiment (Fig. S5), IEPOX was lost to the chamber walls in our reactive uptake experiments. Previous studies have stated that the extent of vapor wall loss is likely a function of the chamber walls' history (Bian et al., 2015; Zhang et al., 2015), and that IEPOX loss to chamber walls that have previously been in contact with acidified seed aerosols may potentially be substantial (Paulot et al., 2009b). The chambers used in this study have been used extensively in previous chamber studies and have been in contact with acidified seed aerosols. It is possible that a larger amount of IEPOX was lost to the chamber walls in "IEPOX first" experiments compared to the "seed aerosols first" experiments, thus causing a higher gas-phase $C_5H_{10}O_3$ signal measured at the end of the "seed aerosols first" experiment compared to the $C_5H_{10}O_3$ signals measured prior to and after the addition of seed aerosols in the "IEPOX first" experiment. Second, it is possible that larger quantities of 3-methyltetrahydrofuran-2,4-diols were formed in "seed aerosols first" experiments compared to "IEPOX first" experiments. This possibility would differ from findings from a recent study by Watanabe et al. (2018) who compared the formation pathways of 3-methyltetrahydrofuran-2,4-diols and 2-methyltetrols in bulk condensed-phase IEPOX reactions. The authors found that condensed-phase isomerization reactions were slower than nucleophilic addition reactions, which led them to conclude that 3-methyltetrahydrofuran-2,4-diol formation might be restricted to low aerosol water content situations. This second possibility would suggest that 3-methyltetrahydrofuran-2,4-diols are still formed in humid conditions even if isomerization reactions are slow. Additional studies utilizing newly constructed chambers and more sophisticated analytical methods (e.g., ion mobility) to resolve structural $C_5H_{10}O_3$ isomers are needed to examine the likelihood of these two possibilities.

A series of "IEPOX first" experiments using seed aerosols of different aerosol acidity was performed to investigate the effect of sulfate mass concentration on SOA formation from the reactive uptake of IEPOX (experiments 3 to 6). In each experiment, IEPOX was injected into the chamber followed by multiple injections of seed aerosols after the HR-ToF-CIMS signals of gas-phase species had stabilized. Each injection of seed aerosols led to an increase in the SOA mass concentration (Fig. S6). Higher SOA mass concentrations were formed in experiments that utilized acidified seed aerosols. Figure 2 shows the dependence of SOA mass concentration on the sulfate mass concentration of seed aerosols of different aerosol acidity. If IEPOX loss to the chamber walls were substantial in these "IEPOX first" experiments, then the SOA mass

concentrations shown in Fig. 2 likely represent lower limits. It should be noted that the sulfate mass concentrations reported for "IEPOX first" experiments were the sums of inorganic sulfate (contributed by seed aerosols) and organic sulfate (formed from IEPOX reactive uptake). A recent study reported that the HR-ToF-AMS ionization efficiencies of inorganic and organic sulfates can be different (Chen et al., 2019). The authors reported that the ionization efficiencies of methanesulfonic acid and ethyl sulfate (two different types of organic sulfates) are ~67 % of that of ammonium sulfate. Since we do not know the ionization efficiencies and mass fractions of organic sulfates formed from IEPOX reactive uptake in our experiments, for simplicity, we assumed that the ionization efficiencies of inorganic and organic sulfates are the same in this work. While this simplified assumption will affect the absolute sulfate mass concentrations reported in this work, we do not expect it to affect our overall conclusion that both sulfate mass and aerosol acidity enhance SOA formation.

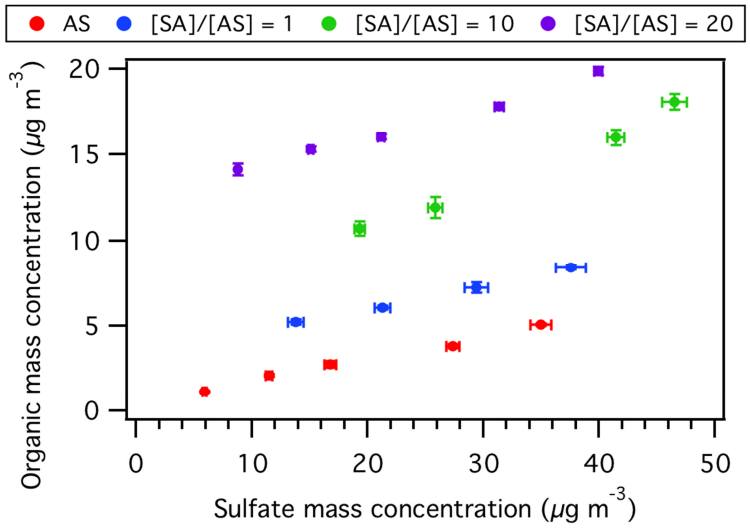

Figure 2: Results from "IEPOX first" experiments using inorganic sulfate seed aerosols of different aerosol acidity (experiments 3 to 6 in Table 1): dependence of the organic mass concentration on sulfate mass concentration. Each set of different colored symbols represents measurements made during an experiment. Each experiment involved multiple injections of seed aerosols into the chamber filled with IEPOX. Aerosol organic and sulfate mass concentrations (20 min averaged) shown here are measured values when the maximum amount of SOA is formed after each injection of seed aerosols in the experiment. Error bars denote one standard deviation across the 20 min measurements. Note that the sulfate mass concentrations reported here are the sums of inorganic and organic sulfate. See text for details.

The enhancement in SOA formation with aerosol acidity was consistent with previous laboratory studies (Surratt et al., 2007b; Lin et al., 2012; Gaston et al., 2014; Kuwata et al., 2015;

Riedel et al., 2016; Nestorowicz et al., 2018; Zhang et al., 2018). The continued increase in SOA mass concentration with each injection of seed aerosols was ubiquitous and was observed in experiments using acidified and non-acidified seed aerosols.

Our finding that sulfate mass enhances IEPOX-derived SOA formation for both highly acidic and less acidic seed aerosols have important implications for previous laboratory studies. Many of these studies reported that aerosol acidity enhances IEPOX reactive uptake, and consequently SOA formation (Surratt et al., 2007b; Lin et al., 2012; Gaston et al., 2014; Kuwata et al., 2015; Riedel et al., 2016). It is possible that some of these previous results can also be explained in the context of sulfate. For example, in their study on isoprene photooxidation in the presence of SO_2, Lewandowski et al. (2015) showed that SOA mass concentration increased with sulfate acidity. However, we found that their measured SOA mass concentrations also showed positive correlation with sulfate mass concentrations, thus indicating that sulfate likely played a role in SOA formation (in addition to aerosol acidity) in their study.

Sulfate mass enhancement is known to increase aerosol acidity, water, surface area and volume, which together facilitate the multiphase chemistry of IEPOX via the heterogeneous uptake rate and particle-phase reaction rates (Xu et al., 2016). However, the poor correlation between isoprene-derived SOA and aerosol water observed in field studies was due to the trade-off effects of aerosol water, which increased aerosol surface area and volume but also decreased particle-phase reaction rates due to the dilution of particle-phase nucleophiles (Budisulistiorini et al., 2013; Budisulistiorini et al., 2015; Xu et al., 2015a). In the Southeastern U.S., while particle-phase reaction rates were enhanced when aerosol acidity was increased, these reaction rates were usually not fast enough to explain the enhanced isoprene-derived SOA formation observed in field studies (Xu et al., 2016). Instead, the strong correlation between isoprene-derived SOA and sulfate mass was hypothesized to be due to sulfate mass mediating SOA formation via the aerosol surface area (or volume) due to the kinetics of SOA formation being limited by aerosol surface area (or aerosol volume) (Lin et al., 2013; Riva et al., 2016; Xu et al., 2016; Budisulistiorini et al., 2017; Zhang et al., 2018).

In our experiments involving multiple seed aerosol injections, the aerosol surface area and volume concentrations increased with each injection of seed aerosols. Thus, the results shown in Fig. 2 also demonstrated that the SOA mass concentration increased with aerosol

surface area and volume concentrations (Fig. S7), which is in agreement with previous hypotheses that sulfate mass can mediate ambient IEPOX-derived SOA formation via aerosol surface area or volume (Lin et al., 2013; Riva et al., 2016; Xu et al., 2016; Budisulistiorini et al., 2017). Experimental limitations prevented us from determining if the SOA formation chemistry was a surface area-limited or a volume-limited process and how this may potentially change with reaction conditions since the measured aerosol surface area and volume concentrations were comprised of inorganic seed aerosols and SOA. A full understanding of the kinetics of IEPOX-derived SOA formation will require laboratory studies that systematically examine the effect of varying aerosol surface area concentrations at a fixed aerosol volume concentration (and vice versa) on SOA formation.

HR-ToF-AMS mass spectra of SOA formed in "IEPOX first" experiments are shown in Fig. 3. The mass spectra have prominent peaks at $C_5H_6O^+$ (*m/z* 82) and $C_4H_5^+$ (*m/z* 53). These ions were also present in ambient isoprene-derived SOA mass spectra resolved by positive matrix factorization (PMF) analysis (Robinson et al., 2011; Slowik et al., 2011; Lin et al., 2012; Budisulistiorini et al., 2013; Chen et al., 2015; Hu et al., 2015; Liu et al., 2015; Xu et al., 2015a; Xu et al., 2015b; Xu et al., 2016). Previous field studies have used the fraction of $C_5H_6O^+$ (*m/z* 82) to the total organic ion signal (f_{C5H6O+}) as a marker ion in the interpretation of ambient data (Robinson et al., 2011; Hu et al., 2015; Liu et al., 2015; Xu et al., 2015b). We found that the f_{C5H6O+} did not differ significantly for SOA formed in these experiments, with values ranging from 1.8 % (Fig. 3a) to 2.3 % (Fig. 3d). This range was similar to values reported for isoprene-derived SOA in previous field studies (Robinson et al., 2011; Slowik et al., 2011; Budisulistiorini et al., 2013; Chen et al., 2015; Hu et al., 2015; Xu et al., 2015b). Figure S8 presents correlation plots between the mass spectra of SOA formed in "IEPOX first" experiments and the PMF factor for isoprene-derived SOA obtained during the SOAS campaign (Xu et al., 2015a). There was generally close clustering along the 1:1 line in the correlation plots. Signals at *m/z* 28 and 44 were lower for the laboratory data, thus suggesting that the laboratory aerosols were less aged than ambient isoprene-derived SOA (Ng et al., 2010).

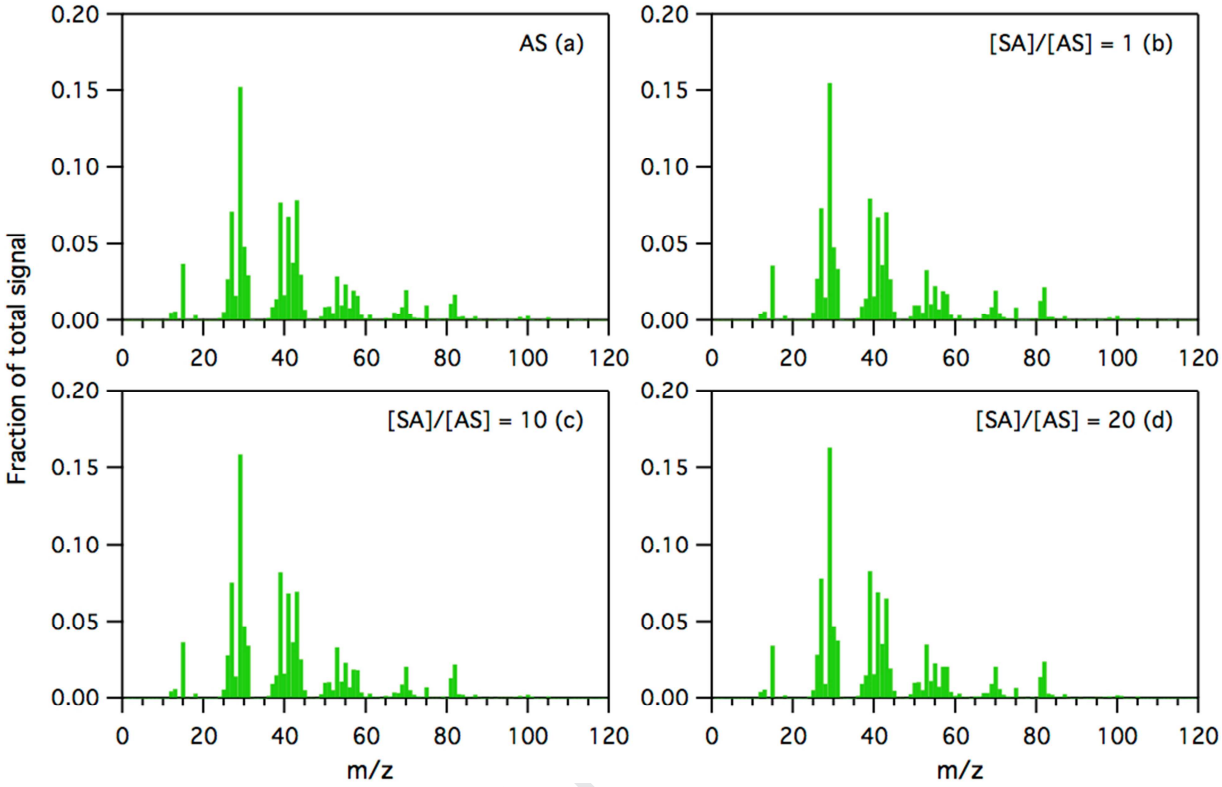

Figure 3: Normalized HR-ToF-AMS mass spectra of SOA formed from the reactive uptake of *trans*-β-IEPOX onto inorganic sulfate seed aerosols during "IEPOX first" experiments. These experiments are conducted using (a) AS, (b) [SA]/[AS] = 1, (c) [SA]/[AS] = 10, and (d) [SA]/[AS] = 20 seed aerosols.

Previous chamber studies that investigated SOA formation from the reactive uptake of IEPOX introduced seed aerosols into the chamber before IEPOX (Lin et al., 2012; Nguyen et al., 2014; Nestorowicz et al., 2018). Hence, we performed a series of "IEPOX first" and "seed aerosols first" experiments using [SA]/[AS] = 10 seed aerosols to investigate how SOA formation depends on the injection order of IEPOX and seed aerosols (experiments 1 to 2, 7 to 10). Unlike the experiments aimed at studying the dependence of SOA formation on sulfate mass concentration (experiments 3 to 6), seed aerosols were injected only once into the chamber before or after the injection of IEPOX in experiments aimed at investigating the effect of injection order. Figure 4 shows that the SOA mass concentration increased with sulfate mass concentration in both the "IEPOX first" and "seed aerosols first" experiments. However, for any given sulfate mass concentration, higher SOA mass concentrations were formed in "seed aerosols first" experiments compared to "IEPOX first" experiments. This indicated that the

416 injection order of IEPOX and seed aerosols in chamber experiments can significantly affect SOA
417 formation.

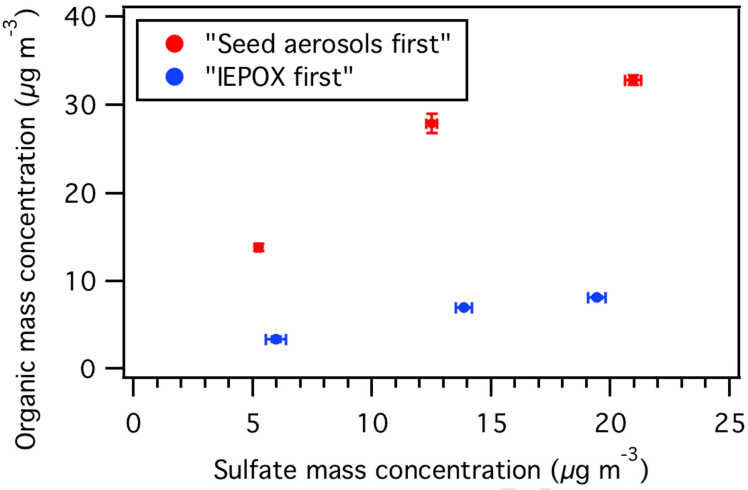

418

419 **Figure 4:** Results from "IEPOX first" and "seed aerosols first" experiments using [SA]/[AS] =
420 10 seed aerosols (experiments 1 to 2, 7 to 10 in Table 1): dependence of the organic mass
421 concentration on sulfate mass concentration. In these experiments, seed aerosols are injected
422 only once into the chamber before ("seed aerosols first", red symbols) or after ("IEPOX first",
423 blue symbols) the injection of IEPOX. Each symbol represents the aerosol organic and sulfate
424 mass concentrations (20 min averaged) measured when the maximum amount of SOA is formed
425 during an experiment. Error bars denote one standard deviation across the 20 min measurements.
426 Note that the sulfate mass concentrations reported for "IEPOX first" experiments are the sums of
427 inorganic and organic sulfate (see text for details), while the sulfate mass concentrations reported
428 for "seed aerosols first" experiments are for inorganic sulfate only.

429 One possibility for the differences in SOA mass concentrations is that a larger amount of
430 IEPOX was lost to the chamber walls in "IEPOX first" experiments compared to the "seed
431 aerosols first" experiments. This would result in higher IEPOX concentrations in "seed aerosols
432 first" experiments (and consequently higher SOA mass concentrations formed) despite the same
433 amount of IEPOX injected into the chamber in both sets of experiments. The second possibility
434 is that different quantities and/or types of particle-phase products were formed in "IEPOX first"
435 and "seed aerosols first" experiments. This possibility was investigated by first comparing the
436 HR-ToF-AMS mass spectra of SOA formed in "IEPOX first" experiments to mass spectra of
437 SOA formed in "seed aerosols first" experiments (Fig. S9). The f_{C5H6O+} did not differ
438 significantly between the two sets of mass spectra. The f_{C5H6O+} ranged between 2.4 % and 2.5 %
439 for SOA formed in "IEPOX first" experiments (Figs. S9a, S9c and S9e), and between 2.3 % and
440 2.5 % for SOA formed in "seed aerosol first" experiments (Figs. S9b, S9d and S9f), within the

441 range of values reported for isoprene-derived SOA in previous field studies (Robinson et al.,
442 2011; Hu et al., 2015; Liu et al., 2015; Xu et al., 2015b). Correlation plots between HR-ToF-
443 AMS mass spectra of SOA formed in "IEPOX first" and "seed aerosols first" experiments (Fig.
444 S10) showed that despite substantial differences in SOA mass concentrations formed, the mass
445 spectra of SOA formed were generally similar.

446 FIGAERO-CIMS measurements were used to gain more insights into the molecular
447 composition and volatilities of particle-phase products formed during "IEPOX first" and "seed
448 aerosols first" experiments. Figures 5 and S11 show the thermograms for $C_5H_{10}O_3$ and $C_5H_{12}O_4$,
449 the two largest signals of particle-phase products measured by the FIGAERO-CIMS
450 (experiments 1 and 2). $C_5H_{10}O_3$ and $C_5H_{12}O_4$ are known tracers of ambient IEPOX-derived SOA
451 (Lopez-Hilfiker et al., 2016). The thermograms for $C_5H_{10}O_3$ and $C_5H_{12}O_4$ contained multiple
452 peaks, which were likely due to the thermal decomposition of higher molecular weight particle-
453 phase compounds during the desorption process to produce the detected molecular fragments
454 (Lopez-Hilfiker et al., 2014; Lopez-Hilfiker et al., 2015). Multi-modal thermograms were also
455 reported for $C_5H_{10}O_3$ and $C_5H_{12}O_4$ components in isoprene-derived SOA measured during the
456 SOAS campaign (Lopez-Hilfiker et al., 2016). To obtain volatility information of particle-phase
457 compounds desorbing (or fragmenting) from the particle collection filter in our experiments, we
458 fitted the total thermograms for $C_5H_{10}O_3$ and $C_5H_{12}O_4$ using a variable number of thermogram
459 peaks of variable peak shape widths and heights. The T_{max} value of each fitted thermogram peak
460 was then compared to the calibration desorption temperature axis (Fig. S4) to estimate the vapor
461 pressures of these desorbed (or fragmented) compounds.

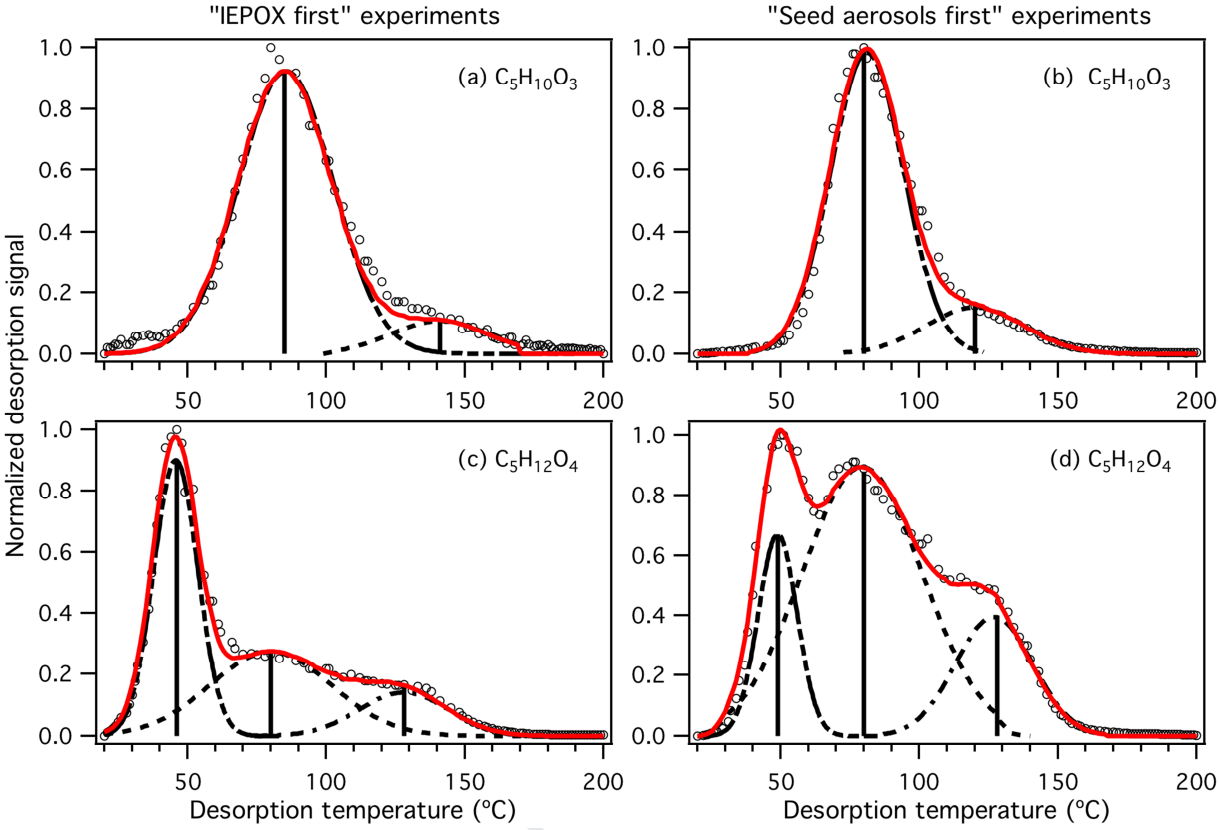

Figure 5: FIGAERO-CIMS thermograms for $C_5H_{10}O_3$ and $C_5H_{12}O_4$ from SOA sampled during (a and c) an "IEPOX first" experiment (experiment 1 in Table 1), and (b and d) a "seed aerosols first" experiment (experiment 2 in Table 1) using [SA]/[AS] = 10 seed aerosols. Thermogram fits are shown in black dashed lines. Red solid lines show the summed thermogram fits. Back solid lines indicate the T_{max} of the fits.

The thermograms for $C_5H_{10}O_3$ from SOA sampled in "IEPOX first" and "seed aerosols first" experiments were best fit to two modes. For $C_5H_{10}O_3$ thermograms measured in "IEPOX first" experiments, the first mode occurred at T_{max} ~85 °C while the second mode occurred at T_{max} ~140 °C (Fig. 5a). For $C_5H_{10}O_3$ thermograms measured in "seed aerosols first" experiments, the two modes occurred at T_{max} ~80 and ~120 °C (Fig. 5b). The most prominent modes in both $C_5H_{10}O_3$ thermograms have a T_{max} at nearly the same temperature (i.e., ~85 and ~80 °C). Since authentic standards for 3-methyltetrahydrofuran-2,4-diols and 2-methyltetrols were not commercially available, we estimated their T_{max} values based on vapor pressures reported in the literature (Lopez-Hilfiker et al., 2016), or calculated from structure activity relationships (Capouet and Muller, 2006) and the calibration desorption temperature axis. The T_{max} values for 3-methyltetrahydrofuran-2,4-diols were expected to be <50 °C based on their estimated vapor

pressures. However, there were no prominent modes present at T_{max} <50 °C in the $C_5H_{10}O_3$ thermograms, which suggested that 3-methyltetrahydrofuran-2,4-diols were present in low quantities in the particle phase. Together, the $C_5H_{10}O_3$ thermograms and gas-phase measurements (Figs. 1a and 1b) suggested that 3-methyltetrahydrofuran-2,4-diols were likely present largely in the gas phase. The modes present at T_{max} = 80 °C and higher temperatures corresponded to vapor pressures that were at least 3 orders of magnitude lower than the estimated vapor pressures of 3-methyltetrahydrofuran-2,4-diols, and were likely caused by molecular fragments of low volatility particle-phase products (Lopez-Hilfiker et al., 2016). The T_{max}'s of the $C_5H_{10}O_3$ thermograms indicated that products with vapor pressures ~10^{-6} Pa and ~10^{-10} Pa were formed in "IEPOX first" experiments, while products with vapor pressures ~10^{-6} Pa and ~10^{-9} Pa were formed in "seed aerosols first" experiments.

The $C_5H_{12}O_4$ thermograms measured in "IEPOX first" and "seed aerosols first" experiments were both best fit to three modes with T_{max} values of ~50, ~80 and ~130 °C (Figs. 4c and 4d). The T_{max} of the first mode (~50 °C) in both $C_5H_{12}O_4$ thermograms corresponded to vapor pressure ~6 x 10^{-4} Pa, which is close to the estimated vapor pressure (~1 x 10^{-4} Pa) calculated from structure activity relationships (Capouet and Muller, 2006). In addition, Lopez-Hilfiker et al. (2016) previously showed that synthesized 2-methyltetrol standards produced unimodal $C_5H_{12}O_4$ thermograms with T_{max} ~55 °C in FIGAERO-CIMS measurements. Hence, the mode at ~50 °C can be tentatively assigned to 2-methyltetrol products. The remaining two modes with T_{max} values ~80 and ~130 °C were likely caused by molecular fragments of low volatility particle-phase products (Lopez-Hilfiker et al., 2016). The T_{max}'s of the $C_5H_{12}O_4$ thermograms indicated that products with vapor pressures ~10^{-6} Pa and ~10^{-9} Pa were formed in "IEPOX first" and "seed aerosols first" experiments.

Since $C_5H_{10}O_3$ and $C_5H_{12}O_4$ contributed to majority of the particle-phase ion signals (~99 %), we assumed that most of the particle-phase products desorbed and/or fragmented to produce these two ions. Based on this assumption, the $C_5H_{10}O_3$ and $C_5H_{12}O_4$ thermograms can then be used to compare the volatility distribution of particle-phase products formed in "IEPOX first" and "seed aerosols first" experiments. Differences in the $C_5H_{10}O_3$ and $C_5H_{12}O_4$ thermogram profiles measured in "IEPOX first" and "seed aerosols first" experiments indicated that the compositional and volatility distribution of particle-phase products formed in these experiments

were different. For example, the T_{max} of the second mode present in $C_5H_{10}O_3$ thermograms were different (i.e., ~140 °C for "IEPOX first" experiment vs. ~120 °C for "seed aerosols first" experiment), which suggested that different products were formed. In addition, the $C_5H_{12}O_4$ thermograms had significantly different desorption profiles. The first mode (T_{max} ~50 °C) had the highest signal in $C_5H_{12}O_4$ thermograms measured in "IEPOX first" experiments, which indicated that 2-methyltetrols were likely the most dominant component of the measured particle-phase $C_5H_{12}O_4$ species. In contrast, the second and third modes (T_{max} ~80 and ~130 °C) were more prominent in $C_5H_{12}O_4$ thermograms measured in "seed aerosols first" experiments, which indicated that the SOA formed in these experiments likely contained larger quantities of low volatility particle-phase products such as oligomers of methyltetrol and hydroxy sulfate ester. We were unable to test this hypothesis since these low volatility products were not commercially available. However, Lopez-Hilfilker et al., (2016) previously showed that a synthesized IEPOX-derived organosulfate $C_5H_{12}SO_7$ thermally decomposed into $C_5H_{10}O_3$ and $C_5H_{12}O_4$ in FIGAERO-CIMS measurements, and the T_{max}'s of prominent modes in the resulting $C_5H_{10}O_3$ and $C_5H_{12}O_4$ thermograms were between 90 and 150 °C. The T_{max}'s of modes contributed by low volatility products observed in this study fell within the temperature range reported by Lopez-Hilfilker et al., (2016).

Comparisons of the raw desorption signals of the $C_5H_{10}O_3$ and $C_5H_{12}O_4$ thermograms (Fig. S11) indicated that "seed aerosols first" experiments produced larger quantities of semi-volatile and low volatility particle-phase products. The formation of larger quantities of semi-volatile and low volatility products in "seed aerosols first" experiments suggested that the rates of particle-phase reactions that form these products were accelerated in cases where seed aerosols were injected into the chamber first followed by IEPOX. Differences in mixing conditions caused by the different timescales at which IEPOX and seed aerosols were introduced into a well-mixed chamber likely affected IEPOX multiphase chemistry. In the case of "seed aerosols first" experiments, IEPOX was injected slowly over a ~2.5 h period into a chamber containing seed aerosols. In contrast, seed aerosols were introduced more quickly (10 to 45 min, depending on the amount of seed aerosols) into an IEPOX-containing chamber in "IEPOX first" experiments.

The exact mechanism by which mixing conditions and timescales in the chamber caused differences in particle-phase reactions rates is currently unknown. One possible explanation is the presence (or absence) of an organic coating around seed aerosols in these experiments. Previous studies showed that the presence of organic coatings on seed aerosols can impede the reactive uptake of IEPOX, and consequently SOA formation (Gaston et al., 2014; Riva et al., 2016; Zhang et al., 2018). We hypothesize that the relatively quick injection of seed aerosols into a chamber filled with IEPOX in "IEPOX first" experiments may have resulted in the rapid formation of an organic coating comprised of IEPOX-derived SOA around the seed aerosols, thus impeding further reactive uptake of IEPOX and SOA formation (Zhang et al., 2018). For "seed aerosols first" experiments, the formation of an organic coating around seed aerosols was likely slower because it took time for the slowly injected IEPOX to equilibrate in the chamber, and hence a longer period of time for the injected IEPOX to diffuse into the seed aerosols and interact with the sulfate to form products. Consequently, the absence of an organic coating allowed more IEPOX uptake by the seed aerosols, resulting in higher SOA mass concentrations formed. Future laboratory studies are warranted to investigate the morphology and mixing state of SOA formed in experiments with different methodologies (e.g., microscopy), as well as modeling studies on possible vapor wall loss, the mixing conditions and timescales (e.g., reaction vs. diffusion) in the chamber during these experiments.

4. Conclusions

The role of inorganic sulfate in SOA formation arising from the reactive uptake of IEPOX at 50 to 56 % RH was investigated in this chamber study. The first part of the study focused on how sulfate mass in seed aerosols of different acidity affects SOA formation. Measurements of the gas- and particle-phase products and mass concentration of SOA formed from multiple injections of seed aerosols into a chamber filled with IEPOX were performed. The SOA mass concentration and gas-phase HR-ToF-CIMS signal for 2-methyltetrols immediately increased upon the first injection of seed aerosols. This indicated that the reactive uptake of IEPOX and subsequent formation of semi-volatile particle-phase products followed by evaporation to the gas phase was fast. Each injection of seed aerosols led to an increase in SOA mass concentration. The increase in SOA mass concentration with each injection of seed aerosols was observed for both acidified and non-acidified seed aerosols, though higher SOA mass

concentrations were observed in experiments that utilized more acidified seed aerosols. Therefore, IEPOX-derived SOA formation was enhanced by both aerosol acidity and sulfate mass. The SOA enhancement caused by the increase in sulfate mass was likely due to the enhancement in aerosol surface area and volume, which increased the IEPOX reactive uptake and subsequent particle-phase reactions (Lin et al., 2013; Riva et al., 2016; Xu et al., 2016; Budisulistiorini et al., 2017; Zhang et al., 2018).

The second part of the study focused on how the mass concentration, composition and volatilities of IEPOX-derived SOA depended on the injection order of IEPOX and seed aerosols in chamber experiments. Higher SOA mass concentrations were measured in experiments where seed aerosols were introduced into the chamber first, followed by IEPOX. This was due to IEPOX potentially being lost to the chamber walls in "IEPOX first" experiments and SOA formed in "seed aerosols first" experiments being comprised of larger quantities of semi-volatile and low volatility organic matter compared to SOA formed in the "IEPOX first" experiments. These observations demonstrated that the mass concentration, composition and volatilities of IEPOX-derived SOA depended on mixing conditions in the chamber brought about by injection procedure. Additional chamber and modeling studies are needed to elucidate the exact mechanism by which different mixing conditions in a chamber lead to differences in the IEPOX multiphase chemistry.

Our results showed that the mass concentration and composition of IEPOX-derived SOA formed in chamber experiments are sensitive to mixing conditions in the chamber brought about by differences in the injection procedure. In addition, the different mixing conditions in "IEPOX first" and "seed aerosols first" experiments produced significantly different $C_5H_{12}O_4$ thermograms measured by the FIGAERO-CIMS. Lopez-Hilfiker et al. (2016) observed different desorption profiles for the $C_5H_{12}O_4$ thermograms of isoprene-derived SOA during different time periods of the SOAS campaign. It is possible that different mixing conditions occurred at the field site during these time periods, and this may have been one of the contributing factors to the different desorption profiles of $C_5H_{12}O_4$ thermograms measured during the SOAS campaign. It is likely that mixing conditions in these experiments represent two extreme cases of mixing in the atmosphere, and that typical mixing conditions in the atmosphere lie somewhere between these two limiting cases. For example, the "IEPOX first" experiments may describe a scenario where a

plume containing sulfate-rich aerosols is transported into a forested region with large isoprene emissions. Conversely, the "seed aerosols first" experiments may describe a scenario where isoprene-rich air is transported into an urban and industrialized area with substantial concentrations of sulfate-rich aerosols. Nevertheless, our results suggest that modeling studies may need to consider how sulfate-rich aerosols and IEPOX are mixed and interact with one another in order to accurately capture IEPOX-derived SOA composition and volatilities in the atmosphere.

Our results may also have implications for chamber studies on other systems where SOA is formed from chemical reactions occurring within inorganic seed aerosols after the uptake of a reactive gas, such as the reactive uptake of carbonyls, olefins and epoxides onto inorganic seed aerosols (Kroll et al., 2005; Liggio and Li, 2006, 2008; Iinuma et al., 2009; De Haan et al., 2018). These previous studies investigated SOA formation by introducing seed aerosols into the chamber before the reactive gas. It is possible that products of different composition and volatilities would be formed if the injection order of seed aerosols and the reactive gas is switched in these chamber studies. However, the potential loss of the reactive gas to the chamber walls in experiments where the reactive gas is introduced into the chamber first needs to be considered as this can affect the amount of SOA formed.

5. Conflicts of interest

The authors declare no conflict of interest.

6. Acknowledgements

This research was funded by NSF AGS-1455588 awarded to Georgia Institute of Technology. The FIGAERO-HR-ToF-CIMS was purchased with NSF Major Research Instrumentation (MRI) grant 1428738. K.O.B. thanks NSF for a graduate research fellowship (DGE-1148903). We thank Raynold Shenje for preliminary work on the *trans-β*-IEPOX synthesis, and Yunle Chen for assistance with preliminary chamber experiments.

7. References

Andreae, M.O., Afchine, A., Albrecht, R., Holanda, B.A., Artaxo, P., Barbosa, H.M.J., Borrmann, S., Cecchini, M.A., Costa, A., Dollner, M., Futterer, D., Jarvinen, E., Jurkat, T.,

626 Klimach, T., Konemann, T., Knote, C., Kramer, M., Krisna, T., Machado, L.A.T., Mertes, S.,
627 Minikin, A., Pohlker, C., Pohlker, M.L., Poschl, U., Rosenfeld, D., Sauer, D., Schlager, H.,
628 Schnaiter, M., Schneider, J., Schulz, C., Spanu, A., Sperling, V.B., Voigt, C., Walser, A., Wang,
629 J., Weinzierl, B., Wendisch, M., Ziereis, H., 2018. Aerosol characteristics and particle
630 production in the upper troposphere over the Amazon Basin. Atmos. Chem. Phys. 18, 921-961.

631 Atkinson, R., Baulch, D.L., Cox, R.A., Crowley, J.N., Hampson, R.F., Hynes, R.G., Jenkin,
632 M.E., Rossi, M.J., Troe, J., 2006. Evaluated kinetic and photochemical data for atmospheric
633 chemistry: Volume II - gas phase reactions of organic species. Atmos. Chem. Phys. 6, 3625-
634 4055.

635 Bahreini, R., Ervens, B., Middlebrook, A.M., Warneke, C., de Gouw, J.A., DeCarlo, P.F.,
636 Jimenez, J.L., Brock, C.A., Neuman, J.A., Ryerson, T.B., Stark, H., Atlas, E., Brioude, J., Fried,
637 A., Holloway, J.S., Peischl, J., Richter, D., Walega, J., Weibring, P., Wollny, A.G., Fehsenfeld,
638 F.C., 2009. Organic aerosol formation in urban and industrial plumes near Houston and Dallas,
639 Texas. Journal of Geophysical Research-Atmospheres 114, 17.

640 Bates, K.H., Crounse, J.D., St Clair, J.M., Bennett, N.B., Nguyen, T.B., Seinfeld, J.H., Stoltz,
641 B.M., Wennberg, P.O., 2014. Gas Phase Production and Loss of Isoprene Epoxydiols. Journal of
642 Physical Chemistry A 118, 1237-1246.

643 Bertram, T.H., Kimmel, J.R., Crisp, T.A., Ryder, O.S., Yatavelli, R.L.N., Thornton, J.A.,
644 Cubison, M.J., Gonin, M., Worsnop, D.R., 2011. A field-deployable, chemical ionization time-
645 of-flight mass spectrometer. Atmos. Meas. Tech. 4, 1471-1479.

646 Bian, Q., May, A.A., Kreidenweis, S.M., Pierce, J.R., 2015. Investigation of particle and vapor
647 wall-loss effects on controlled wood-smoke smog-chamber experiments. Atmos. Chem. Phys.
648 15, 11027-11045.

649 Boyd, C.M., Sanchez, J., Xu, L., Eugene, A.J., Nah, T., Tuet, W.Y., Guzman, M.I., Ng, N.L.,
650 2015. Secondary organic aerosol formation from the β-pinene+NO3 system: effect of humidity
651 and peroxy radical fate. Atmos. Chem. Phys. 15, 7497-7522.

652 Budisulistiorini, S.H., Canagaratna, M.R., Croteau, P.L., Marth, W.J., Baumann, K., Edgerton,
653 E.S., Shaw, S.L., Knipping, E.M., Worsnop, D.R., Jayne, J.T., Gold, A., Surratt, J.D., 2013.
654 Real-Time Continuous Characterization of Secondary Organic Aerosol Derived from Isoprene
655 Epoxydiols in Downtown Atlanta, Georgia, Using the Aerodyne Aerosol Chemical Speciation
656 Monitor. Environmental Science & Technology 47, 5686-5694.

657 Budisulistiorini, S.H., Li, X., Bairai, S.T., Renfro, J., Liu, Y., Liu, Y.J., McKinney, K.A., Martin,
658 S.T., McNeill, V.F., Pye, H.O.T., Nenes, A., Neff, M.E., Stone, E.A., Mueller, S., Knote, C.,
659 Shaw, S.L., Zhang, Z., Gold, A., Surratt, J.D., 2015. Examining the effects of anthropogenic
660 emissions on isoprene-derived secondary organic aerosol formation during the 2013 Southern
661 Oxidant and Aerosol Study (SOAS) at the Look Rock, Tennessee ground site. Atmos. Chem.
662 Phys. 15, 8871-8888.

663 Budisulistiorini, S.H., Nenes, A., Carlton, A.G., Surratt, J.D., McNeill, V.F., Pye, H.O.T., 2017.
664 Simulating Aqueous-Phase Isoprene-Epoxydiol (IEPOX) Secondary Organic Aerosol Production
665 During the 2013 Southern Oxidant and Aerosol Study (SOAS). Environmental Science &
666 Technology 51, 5026–5034.

667 Canagaratna, M.R., Jimenez, J.L., Kroll, J.H., Chen, Q., Kessler, S.H., Massoli, P., Hildebrandt
668 Ruiz, L., Fortner, E., Williams, L.R., Wilson, K.R., Surratt, J.D., Donahue, N.M., Jayne, J.T.,
669 Worsnop, D.R., 2015. Elemental ratio measurements of organic compounds using aerosol mass
670 spectrometry: characterization, improved calibration, and implications. Atmos. Chem. Phys. 15,
671 253-272.

672 Capouet, M., Muller, J.F., 2006. A group contribution method for estimating the vapour
673 pressures of alpha-pinene oxidation products. Atmos. Chem. Phys. 6, 1455-1467.

674 Carlton, A.G., Wiedinmyer, C., Kroll, J.H., 2009. A review of Secondary Organic Aerosol
675 (SOA) formation from isoprene. Atmos. Chem. Phys. 9, 4987-5005.

676 Chan, M.N., Surratt, J.D., Claeys, M., Edgerton, E.S., Tanner, R.L., Shaw, S.L., Zheng, M.,
677 Knipping, E.M., Eddingsaas, N.C., Wennberg, P.O., Seinfeld, J.H., 2010. Characterization and
678 Quantification of Isoprene-Derived Epoxydiols in Ambient Aerosol in the Southeastern United
679 States. Environmental Science & Technology 44, 4590-4596.

680 Chen, Q., Farmer, D.K., Rizzo, L.V., Pauliquevis, T., Kuwata, M., Karl, T.G., Guenther, A.,
681 Allan, J.D., Coe, H., Andreae, M.O., Poschl, U., Jimenez, J.L., Artaxo, P., Martin, S.T., 2015.
682 Submicron particle mass concentrations and sources in the Amazonian wet season (AMAZE-08).
683 Atmos. Chem. Phys. 15, 3687-3701.

684 Chen, Y., Xu, L., Humphry, T., Hettiyadura, A.P.S., Ovadnevaite, J., Huang, S., Poulain, L.,
685 Schroder, J.C., Campuzano-Jost, P., Jimenez, J.L., Herrmann, H., O'Dowd, C., Stone, E.A., Ng,
686 N.L., 2019. Response of the Aerodyne Aerosol Mass Spectrometer to Inorganic Sulfates and
687 Organosulfur Compounds: Applications in Field and Laboratory Measurements. Environmental
688 Science & Technology 53, 5176-5186.

689 Cui, T., Zeng, Z., dos Santos, E.O., Zhang, Z., Chen, Y., Zhang, Y., Rose, C.A., Budisulistiorini,
690 S.H., Collins, L.B., Bodnar, W.M., de Souza, R.A.F., Martin, S.T., Machado, C.M.D., Turpin,
691 B.J., Gold, A., Ault, A.P., Surratt, J.D., 2018. Development of a hydrophilic interaction liquid
692 chromatography (HILIC) method for the chemical characterization of water-soluble isoprene
693 epoxydiol (IEPOX)-derived secondary organic aerosol. Environmental Science: Processes &
694 Impacts 20, 1524-1536.

695 De Haan, D.O., Jimenez, N.G., de Loera, A., Cazaunau, M., Gratien, A., Pangui, E., Doussin,
696 J.F., 2018. Methylglyoxal Uptake Coefficients on Aqueous Aerosol Surfaces. Journal of Physical
697 Chemistry A 122, 4854-4860.

698 DeCarlo, P.F., Kimmel, J.R., Trimborn, A., Northway, M.J., Jayne, J.T., Aiken, A.C., Gonin, M.,
699 Fuhrer, K., Horvath, T., Docherty, K.S., Worsnop, D.R., Jimenez, J.L., 2006. Field-deployable,
700 high-resolution, time-of-flight aerosol mass spectrometer. Analytical Chemistry 78, 8281-8289.

701 Docherty, K.S., Jaoui, M., Corse, E., Jimenez, J.L., Offenberg, J.H., Lewandowski, M.,
702 Kleindienst, T.E., 2013. Collection Efficiency of the Aerosol Mass Spectrometer for Chamber-
703 Generated Secondary Organic Aerosols. Aerosol Science and Technology 47, 294-309.

704 Eddingsaas, N.C., VanderVelde, D.G., Wennberg, P.O., 2010. Kinetics and Products of the
705 Acid-Catalyzed Ring-Opening of Atmospherically Relevant Butyl Epoxy Alcohols. Journal of
706 Physical Chemistry A 114, 8106-8113.

Fountoukis, C., Nenes, A., 2007. ISORROPIA II: a computationally efficient thermodynamic equilibrium model for K+-Ca2+-Mg2+-Nh(4)(+)-Na+-SO42--NO3--Cl--H2O aerosols. Atmos. Chem. Phys. 7, 4639-4659.

Gaston, C.J., Riedel, T.P., Zhang, Z.F., Gold, A., Surratt, J.D., Thornton, J.A., 2014. Reactive Uptake of an Isoprene-Derived Epoxydiol to Submicron Aerosol Particles. Environmental Science & Technology 48, 11178-11186.

Guenther, A.B., Jiang, X., Heald, C.L., Sakulyanontvittaya, T., Duhl, T., Emmons, L.K., Wang, X., 2012. The Model of Emissions of Gases and Aerosols from Nature version 2.1 (MEGAN2.1): an extended and updated framework for modeling biogenic emissions. Geoscientific Model Development 5, 1471-1492.

Guo, H., Xu, L., Bougiatioti, A., Cerully, K.M., Capps, S.L., Hite Jr, J.R., Carlton, A.G., Lee, S.H., Bergin, M.H., Ng, N.L., Nenes, A., Weber, R.J., 2015. Fine-particle water and pH in the southeastern United States. Atmos. Chem. Phys. 15, 5211-5228.

Hu, W.W., Campuzano-Jost, P., Palm, B.B., Day, D.A., Ortega, A.M., Hayes, P.L., Krechmer, J.E., Chen, Q., Kuwata, M., Liu, Y.J., de Sa, S.S., McKinney, K., Martin, S.T., Hu, M., Budisulistiorini, S.H., Riva, M., Surratt, J.D., St Clair, J.M., Isaacman-Van Wertz, G., Yee, L.D., Goldstein, A.H., Carbone, S., Brito, J., Artaxo, P., de Gouw, J.A., Koss, A., Wisthaler, A., Mikoviny, T., Karl, T., Kaser, L., Jud, W., Hansel, A., Docherty, K.S., Alexander, M.L., Robinson, N.H., Coe, H., Allan, J.D., Canagaratna, M.R., Paulot, F., Jimenez, J.L., 2015. Characterization of a real-time tracer for isoprene epoxydiols-derived secondary organic aerosol (IEPOX-SOA) from aerosol mass spectrometer measurements. Atmos. Chem. Phys. 15, 11807-11833.

Iinuma, Y., Boge, O., Kahnt, A., Herrmann, H., 2009. Laboratory chamber studies on the formation of organosulfates from reactive uptake of monoterpene oxides. Physical Chemistry Chemical Physics 11, 7985-7997.

Kroll, J.H., Ng, N.L., Murphy, S.M., Varutbangkul, V., Flagan, R.C., Seinfeld, J.H., 2005. Chamber studies of secondary organic aerosol growth by reactive uptake of simple carbonyl compounds. Journal of Geophysical Research-Atmospheres 110, 10.

735 Kuwata, M., Liu, Y., McKinney, K., Martin, S.T., 2015. Physical state and acidity of inorganic
736 sulfate can regulate the production of secondary organic material from isoprene photooxidation
737 products. Physical Chemistry Chemical Physics 17, 5670-5678.

738 Lee, B.H., Lopez-Hilfiker, F.D., Mohr, C., Kurten, T., Worsnop, D.R., Thornton, J.A., 2014. An
739 Iodide-Adduct High-Resolution Time-of-Flight Chemical-Ionization Mass Spectrometer:
740 Application to Atmospheric Inorganic and Organic Compounds. Environmental Science &
741 Technology 48, 6309-6317.

742 Lelieveld, J., Butler, T.M., Crowley, J.N., Dillon, T.J., Fischer, H., Ganzeveld, L., Harder, H.,
743 Lawrence, M.G., Martinez, M., Taraborrelli, D., Williams, J., 2008. Atmospheric oxidation
744 capacity sustained by a tropical forest. Nature 452, 737-740.

745 Lewandowski, M., Jaoui, M., Offenberg, J.H., Krug, J.D., Kleindienst, T.E., 2015. Atmospheric
746 oxidation of isoprene and 1,3-butadiene: influence of aerosol acidity and relative humidity on
747 secondary organic aerosol. Atmos. Chem. Phys. 15, 3773-3783.

748 Liggio, J., Li, S.M., 2006. Reactive uptake of pinonaldehyde on acidic aerosols. Journal of
749 Geophysical Research-Atmospheres 111, 12.

750 Liggio, J., Li, S.M., 2008. Reversible and irreversible processing of biogenic olefins on acidic
751 aerosols. Atmos. Chem. Phys. 8, 2039-2055.

752 Lin, Y.H., Knipping, E.M., Edgerton, E.S., Shaw, S.L., Surratt, J.D., 2013. Investigating the
753 influences of SO2 and NH3 levels on isoprene-derived secondary organic aerosol formation
754 using conditional sampling approaches. Atmos. Chem. Phys. 13, 8457-8470.

755 Lin, Y.H., Zhang, Z.F., Docherty, K.S., Zhang, H.F., Budisulistiorini, S.H., Rubitschun, C.L.,
756 Shaw, S.L., Knipping, E.M., Edgerton, E.S., Kleindienst, T.E., Gold, A., Surratt, J.D., 2012.
757 Isoprene Epoxydiols as Precursors to Secondary Organic Aerosol Formation: Acid-Catalyzed
758 Reactive Uptake Studies with Authentic Compounds. Environmental Science & Technology 46,
759 250-258.

760 Liu, Y.J., Kuwata, M., Strick, B.F., Geiger, F.M., Thomson, R.J., McKinney, K.A., Martin, S.T.,
761 2015. Uptake of Epoxydiol Isomers Accounts for Half of the Particle-Phase Material Produced

762 from Isoprene Photooxidation via the HO2 Pathway. Environmental Science & Technology 49,
763 250-258.

764 Lopez-Hilfiker, F.D., Mohr, C., D'Ambro, E.L., Lutz, A., Riedel, T.P., Gaston, C.J., Iyer, S.,
765 Zhang, Z., Gold, A., Surratt, J.D., Lee, B.H., Kurten, T., Hu, W.W., Jimenez, J., Hallquist, M.,
766 Thornton, J.A., 2016. Molecular Composition and Volatility of Organic Aerosol in the
767 Southeastern US: Implications for IEPOX Derived SOA. Environmental Science & Technology
768 50, 2200-2209.

769 Lopez-Hilfiker, F.D., Mohr, C., Ehn, M., Rubach, F., Kleist, E., Wildt, J., Mentel, T.F.,
770 Carrasquillo, A.J., Daumit, K.E., Hunter, J.F., Kroll, J.H., Worsnop, D.R., Thornton, J.A., 2015.
771 Phase partitioning and volatility of secondary organic aerosol components formed from alpha-
772 pinene ozonolysis and OH oxidation: the importance of accretion products and other low
773 volatility compounds. Atmos. Chem. Phys. 15, 7765-7776.

774 Lopez-Hilfiker, F.D., Mohr, C., Ehn, M., Rubach, F., Kleist, E., Wildt, J., Mentel, T.F., Lutz, A.,
775 Hallquist, M., Worsnop, D., Thornton, J.A., 2014. A novel method for online analysis of gas and
776 particle composition: description and evaluation of a Filter Inlet for Gases and AEROsols
777 (FIGAERO). Atmos. Meas. Tech. 7, 983-1001.

778 Matthew, B.M., Middlebrook, A.M., Onasch, T.B., 2008. Collection efficiencies in an Aerodyne
779 Aerosol Mass Spectrometer as a function of particle phase for laboratory generated aerosols.
780 Aerosol Science and Technology 42, 884-898.

781 Minerath, E.C., Casale, M.T., Elrod, M.J., 2008. Kinetics feasibility study of alcohol sulfate
782 esterification reactions in tropospheric aerosols. Environmental Science & Technology 42, 4410-
783 4415.

784 Mohr, C., Lopez-Hilfiker, F.D., Yli-Juuti, T., Heitto, A., Lutz, A., Hallquist, M., D'Ambro, E.L.,
785 Rissanen, M.P., Hao, L., Schobesberger, S., Kulmala, M., Mauldin, R.L., Makkonen, U., Sipilä,
786 M., Petäjä, T., Thornton, J.A., 2017. Ambient observations of dimers from terpene oxidation in
787 the gas phase: Implications for new particle formation and growth. Geophysical Research Letters
788 44, 2958-2966.

789 Nestorowicz, K., Jaoui, M., Rudzinski, K.J., Lewandowski, M., Kleindienst, T.E., Spolnik, G.,
790 Danikiewicz, W., Szmigielski, R., 2018. Chemical composition of isoprene SOA under acidic
791 and non-acidic conditions: effect of relative humidity. Atmos. Chem. Phys. 18, 18101-18121.

792 Ng, N.L., Canagaratna, M.R., Zhang, Q., Jimenez, J.L., Tian, J., Ulbrich, I.M., Kroll, J.H.,
793 Docherty, K.S., Chhabra, P.S., Bahreini, R., Murphy, S.M., Seinfeld, J.H., Hildebrandt, L.,
794 Donahue, N.M., DeCarlo, P.F., Lanz, V.A., Prevot, A.S.H., Dinar, E., Rudich, Y., Worsnop,
795 D.R., 2010. Organic aerosol components observed in Northern Hemispheric datasets from
796 Aerosol Mass Spectrometry. Atmos. Chem. Phys. 10, 4625-4641.

797 Nguyen, T.B., Coggon, M.M., Bates, K.H., Zhang, X., Schwantes, R.H., Schilling, K.A., Loza,
798 C.L., Flagan, R.C., Wennberg, P.O., Seinfeld, J.H., 2014. Organic aerosol formation from the
799 reactive uptake of isoprene epoxydiols (IEPOX) onto non-acidified inorganic seeds. Atmos.
800 Chem. Phys. 14, 3497-3510.

801 Paulot, F., Crounse, J.D., Kjaergaard, H.G., Kroll, J.H., Seinfeld, J.H., Wennberg, P.O., 2009a.
802 Isoprene photooxidation: new insights into the production of acids and organic nitrates. Atmos.
803 Chem. Phys. 9, 1479-1501.

804 Paulot, F., Crounse, J.D., Kjaergaard, H.G., Kurten, A., St Clair, J.M., Seinfeld, J.H., Wennberg,
805 P.O., 2009b. Unexpected Epoxide Formation in the Gas-Phase Photooxidation of Isoprene.
806 Science 325, 730-733.

807 Rattanavaraha, W., Chu, K., Budisulistiorini, H., Riva, M., Lin, Y.-H., Edgerton, E.S., Baumann,
808 K., Shaw, S.L., Guo, H., King, L., Weber, R.J., Neff, M.E., Stone, E.A., Offenberg, J.H., Zhang,
809 Z., Gold, A., Surratt, J.D., 2016. Assessing the impact of anthropogenic pollution on isoprene-
810 derived secondary organic aerosol formation in PM2.5 collected from the Birmingham,
811 Alabama, ground site during the 2013 Southern Oxidant and Aerosol Study. Atmos. Chem. Phys.
812 16, 4897-4914.

813 Ren, X., Olson, J.R., Crawford, J.H., Brune, W.H., Mao, J., Long, R.B., Chen, Z., Chen, G.,
814 Avery, M.A., Sachse, G.W., Barrick, J.D., Diskin, G.S., Huey, L.G., Fried, A., Cohen, R.C.,
815 Heikes, B., Wennberg, P.O., Singh, H.B., Blake, D.R., Shetter, R.E., 2008. HOx chemistry

816 during INTEX-A 2004: Observation, model calculation, and comparison with previous studies.
817 Journal of Geophysical Research: Atmospheres 113, D05310.

818 Riedel, T.P., Lin, Y.-H., Budisulistiorini, S.H., Gaston, C.J., Thornton, J.A., Zhang, Z., Vizuete,
819 W., Gold, A., Surratt, J.D., 2015. Heterogeneous Reactions of Isoprene-Derived Epoxides:
820 Reaction Probabilities and Molar Secondary Organic Aerosol Yield Estimates. Environmental
821 Science & Technology Letters 2, 38-42.

822 Riedel, T.P., Lin, Y.H., Zhang, Z., Chu, K., Thornton, J.A., Vizuete, W., Gold, A., Surratt, J.D.,
823 2016. Constraining condensed-phase formation kinetics of secondary organic aerosol
824 components from isoprene epoxydiols. Atmos. Chem. Phys. 16, 1245-1254.

825 Riva, M., Bell, D.M., Hansen, A.M.K., Drozd, G.T., Zhang, Z.F., Gold, A., Imre, D., Surratt,
826 J.D., Glasius, M., Zelenyuk, A., 2016. Effect of Organic Coatings, Humidity and Aerosol Acidity
827 on Multiphase Chemistry of Isoprene Epoxydiols. Environmental Science & Technology 50,
828 5580-5588.

829 Robinson, N.H., Hamilton, J.F., Allan, J.D., Langford, B., Oram, D.E., Chen, Q., Docherty, K.,
830 Farmer, D.K., Jimenez, J.L., Ward, M.W., Hewitt, C.N., Barley, M.H., Jenkin, M.E., Rickard,
831 A.R., Martin, S.T., McFiggans, G., Coe, H., 2011. Evidence for a significant proportion of
832 Secondary Organic Aerosol from isoprene above a maritime tropical forest. Atmos. Chem. Phys.
833 11, 1039-1050.

834 Sareen, N., Waxman, E.M., Turpin, B.J., Volkamer, R., Carlton, A.G., 2017. Potential of Aerosol
835 Liquid Water to Facilitate Organic Aerosol Formation: Assessing Knowledge Gaps about
836 Precursors and Partitioning. Environmental Science & Technology 51, 3327-3335.

837 Slowik, J.G., Brook, J., Chang, R.Y.W., Evans, G.J., Hayden, K., Jeong, C.H., Li, S.M., Liggio,
838 J., Liu, P.S.K., McGuire, M., Mihele, C., Sjostedt, S., Vlasenko, A., Abbatt, J.P.D., 2011.
839 Photochemical processing of organic aerosol at nearby continental sites: contrast between urban
840 plumes and regional aerosol. Atmos. Chem. Phys. 11, 2991-3006.

841 St. Clair, J.M., Rivera-Rios, J.C., Crounse, J.D., Knap, H.C., Bates, K.H., Teng, A.P., Jørgensen,
842 S., Kjaergaard, H.G., Keutsch, F.N., Wennberg, P.O., 2016. Kinetics and Products of the

Reaction of the First-Generation Isoprene Hydroxy Hydroperoxide (ISOPOOH) with OH. The Journal of Physical Chemistry A 120, 1441–1451.

Surratt, J.D., Chan, A.W.H., Eddingsaas, N.C., Chan, M.N., Loza, C.L., Kwan, A.J., Hersey, S.P., Flagan, R.C., Wennberg, P.O., Seinfeld, J.H., 2010. Reactive intermediates revealed in secondary organic aerosol formation from isoprene. Proceedings of the National Academy of Sciences of the United States of America 107, 6640-6645.

Surratt, J.D., Gomez-Gonzalez, Y., Chan, A.W.H., Vermeylen, R., Shahgholi, M., Kleindienst, T.E., Edney, E.O., Offenberg, J.H., Lewandowski, M., Jaoui, M., Maenhaut, W., Claeys, M., Flagan, R.C., Seinfeld, J.H., 2008. Organosulfate formation in biogenic secondary organic aerosol. Journal of Physical Chemistry A 112, 8345-8378.

Surratt, J.D., Kroll, J.H., Kleindienst, T.E., Edney, E.O., Claeys, M., Sorooshian, A., Ng, N.L., Offenberg, J.H., Lewandowski, M., Jaoui, M., Flagan, R.C., Seinfeld, J.H., 2007a. Evidence for organosulfates in secondary organic aerosol. Environmental Science & Technology 41, 517-527.

Surratt, J.D., Lewandowski, M., Offenberg, J.H., Jaoui, M., Kleindienst, T.E., Edney, E.O., Seinfeld, J.H., 2007b. Effect of acidity on secondary organic aerosol formation from isoprene. Environmental Science & Technology 41, 5363-5369.

Thornton, J.A., Wooldridge, P.J., Cohen, R.C., Martinez, M., Harder, H., Brune, W.H., Williams, E.J., Roberts, J.M., Fehsenfeld, F.C., Hall, S.R., Shetter, R.E., Wert, B.P., Fried, A., 2002. Ozone production rates as a function of NOx abundances and HOx production rates in the Nashville urban plume. Journal of Geophysical Research: Atmospheres 107, ACH 7-1-ACH 7-17.

Wang, W., Kourtchev, I., Graham, B., Cafmeyer, J., Maenhaut, W., Claeys, M., 2005. Characterization of oxygenated derivatives of isoprene related to 2-methyltetrols in Amazonian aerosols using trimethylsilylation and gas chromatography/ion trap mass spectrometry. Rapid Communications in Mass Spectrometry 19, 1343-1351.

868 Watanabe, A.C., Stropoli, S.J., Elrod, M.J., 2018. Assessing the Potential Mechanisms of
869 Isomerization Reactions of Isoprene Epoxydiols on Secondary Organic Aerosol. Environmental
870 Science & Technology 52, 8346-8354.

871 Weber, R.J., Guo, H.Y., Russell, A.G., Nenes, A., 2016. High aerosol acidity despite declining
872 atmospheric sulfate concentrations over the past 15 years. Nat. Geosci. 9, 282-286.

873 Wennberg, P.O., Bates, K.H., Crounse, J.D., Dodson, L.G., McVay, R.C., Mertens, L.A.,
874 Nguyen, T.B., Praske, E., Schwantes, R.H., Smarte, M.D., St Clair, J.M., Teng, A.P., Zhang, X.,
875 Seinfeld, J.H., 2018. Gas-Phase Reactions of Isoprene and Its Major Oxidation Products.
876 Chemical Reviews 118, 3337-3390.

877 Worton, D.R., Surratt, J.D., LaFranchi, B.W., Chan, A.W.H., Zhao, Y.L., Weber, R.J., Park,
878 J.H., Gilman, J.B., de Gouw, J., Park, C., Schade, G., Beaver, M., St Clair, J.M., Crounse, J.,
879 Wennberg, P., Wolfe, G.M., Harrold, S., Thornton, J.A., Farmer, D.K., Docherty, K.S., Cubison,
880 M.J., Jimenez, J.L., Frossard, A.A., Russell, L.M., Kristensen, K., Glasius, M., Mao, J.Q., Ren,
881 X.R., Brune, W., Browne, E.C., Pusede, S.E., Cohen, R.C., Seinfeld, J.H., Goldsteint, A.H.,
882 2013. Observational Insights into Aerosol Formation from Isoprene. Environmental Science &
883 Technology 47, 11403-11413.

884 Xu, L., Guo, H.Y., Boyd, C.M., Klein, M., Bougiatioti, A., Cerully, K.M., Hite, J.R., Isaacman-
885 VanWertz, G., Kreisberg, N.M., Knote, C., Olson, K., Koss, A., Goldstein, A.H., Hering, S.V.,
886 de Gouw, J., Baumann, K., Lee, S.H., Nenes, A., Weber, R.J., Ng, N.L., 2015a. Effects of
887 anthropogenic emissions on aerosol formation from isoprene and monoterpenes in the
888 southeastern United States. Proceedings of the National Academy of Sciences of the United
889 States of America 112, 37-42.

890 Xu, L., Middlebrook, A.M., Liao, J., de Gouw, J.A., Guo, H.Y., Weber, R.J., Nenes, A., Lopez-
891 Hilfiker, F.D., Lee, B.H., Thornton, J.A., Brock, C.A., Neuman, J.A., Nowak, J.B., Pollack, I.B.,
892 Welti, A., Graus, M., Warneke, C., Ng, N.L., 2016. Enhanced formation of isoprene-derived
893 organic aerosol in sulfur-rich power plant plumes during Southeast Nexus. Journal of
894 Geophysical Research-Atmospheres 121, 11137-11153.

Xu, L., Suresh, S., Guo, H., Weber, R.J., Ng, N.L., 2015b. Aerosol characterization over the southeastern United States using high-resolution aerosol mass spectrometry: spatial and seasonal variation of aerosol composition and sources with a focus on organic nitrates. Atmos. Chem. Phys. 15, 7307-7336.

Zhang, X., Schwantes, R.H., McVay, R.C., Lignell, H., Coggon, M.M., Flagan, R.C., Seinfeld, J.H., 2015. Vapor wall deposition in Teflon chambers. Atmos. Chem. Phys. 15, 4197-4214.

Zhang, Y., Chen, Y., Lambe, A.T., Olson, N.E., Lei, Z., Craig, R.L., Zhang, Z., Gold, A., Onasch, T.B., Jayne, J.T., Worsnop, D.R., Gaston, C.J., Thornton, J.A., Vizuete, W., Ault, A.P., Surratt, J.D., 2018. Effect of the Aerosol-Phase State on Secondary Organic Aerosol Formation from the Reactive Uptake of Isoprene-Derived Epoxydiols (IEPOX). Environmental Science & Technology Letters 5, 167-174.

Zhang, Y.J., Tang, L.L., Sun, Y.L., Favez, O., Canonaco, F., Albinet, A., Couvidat, F., Liu, D.T., Jayne, J.T., Wang, Z., Croteau, P.L., Canagaratna, M.R., Zhou, H.C., Prevot, A.S.H., Worsnop, D.R., 2017. Limited formation of isoprene epoxydiols-derived secondary organic aerosol under NOx-rich environments in Eastern China. Geophysical Research Letters 44, 2035-2043.

Zhang, Z., Lin, Y.H., Zhang, H., Surratt, J.D., Ball, L.M., Gold, A., 2012. Technical Note: Synthesis of isoprene atmospheric oxidation products: isomeric epoxydiols and the rearrangement products cis- and trans-3-methyl-3,4-dihydroxytetrahydrofuran. Atmos. Chem. Phys. 12, 8529-8535.

- SOA formation increased with the sulfate mass for highly and less acidic aerosols.
- More SOA was formed when highly acidic aerosols were used.
- SOA formation depend on IEPOX and seed aerosols injection order in experiments.
- More SOA was formed when seed aerosols were injected into the chamber first.

Declaration of interests

☒ The authors declare that they have no known competing financial interests or personal relationships that could have appeared to influence the work reported in this paper.

☐The authors declare the following financial interests/personal relationships which may be considered as potential competing interests: